Cashew nut testa tannin resin – preparation, characterization and adsorption studies

N. J. Nnaji, N. I. Okafor, A. M. Ekwonu, O. U. Osuji, O. O. Okwukogu, O. Okoye, A. I. Anozie, S. C. Anene, R. C. Ehiri & T. U. Onuegbu

View supplementary material ↗

Published online: 03 Jun 2021.

Submit your article to this journal ↗

View related articles ↗

View Crossmark data ↗

JTUSCI

J of Taibah University for Science Journal

Taylor & Francis
Taylor & Francis Group

Cashew nut testa tannin resin – preparation, characterization and adsorption studies

N. J. Nnaji[a], N. I. Okafor[b], A. M. Ekwonu[c], O. U. Osuji[a], O. O. Okwukogu[d], O. Okoye[d], A. I. Anozie[d], S. C. Anene[e], R. C. Ehiri[a] and T. U. Onuegbu[d]

[a]Department of Chemistry, Alex Ekwueme Federal University Ndufu Alike Ikwo, Abakaliki, Nigeria; [b]School of Pharmacy, Department of Pharmaceutics, University of the Western Cape, Cape Town, South Africa; [c]Department of Chemistry, Anambra State University, Uli, Nigeria; [d]Department of Pure and Industrial Chemistry, Nnamdi Azikiwe University, Awka, Nigeria; [e]Department of Science Laboratory Technology, Institute of Management and Technology, Enugu, Nigeria

ABSTRACT

Adsorption of metal ions and dyes from water by cashew nut testa tannin resin (CATAR) was studied and the effects of temperature, initial pH, initial concentration and time were investigated. Scanning electron microscopy (SEM) and infrared spectroscopy (FTIR) reveal effective adsorption processes. Kinetic studies show that CATAR adsorption is complex and thermodynamic parameters calculated reveal spontaneous and endothermic adsorption of studied pollutants onto CATAR. The use of CATAR as an alternative adsorbent is proposed considering that of simulated wastewaters gave excellent removal performances of 94.0% (Cd ions), 99.4% (Cu ions) and 97.1% (Pb ions) at pH of 6 and 303 K using amount of CATAR. Removal performances obtained for simulated dye wastewaters using CATAR at similar conditions for removal of metal ions gave 71.1%, 79.2% and 86.6%, respectively for crystal violet, methylene blue and malachite green.

1. Introduction

Heavy metals have great importance to human health; therefore, many research interests have been attracted to this area of scholasticism. This is particularly so considering that natural processes and human activities are known to pollute the water in cities and rural areas [1–3]. Copper (Cu), cadmium (Cd) and lead (Pb) are very toxic heavy metals of interest [4,5] as they concern environmental studies. Although cadmium finds wide application in some industrial processes, it is nephrotoxic [6] and causes renal stone formation [7]. Lead application is found in smelting, painting, plumbing and printing industries [8] and as an antiknock agent in petrol, but its use in petrol production is highly discouraged. Studies on lead have revealed that harm is caused to vital body organs and lead to the impairment of psychological and neurobehavioural functions at low levels [9]. Copper is considered an essential element and its deficiency is known to increase adiposity [10], but it is known to cause oxidative stress and consequently induce DNA damage [11].

Industries, such as textile, paper, plastic, cosmetics, rubber, leather tanning, food processing, printing and dye manufacturing, make use of dyes [6]. Consequently, effluents from these industries characterize dye concentrations at undesirable levels. Dyes are generally recalcitrant in nature giving rise to non-biodegradability

property and impact undesirable colour to water bodies causing a decrease in sunlight penetration, which affects aquatic life [6]. Nephrotoxicity of cadmium is known and it causes the formation of renal stone [6,7]. Lead is deposited in the environment by industrial activities and high exposure levels damage vital body organs. However, low levels impair psychological and neurobehavioural functions [8]. Excess accumulation of copper is detrimental to health [12]. Malachite green toxicity is detrimental to health and particularly destroys the nervous system, brain, liver and decreases growth and fertility rates amongst others [13]. Exposure of one to methylene blue at elevated levels is harmful to the body [14]. Crystal violet is a biohazardous substance, which by in-vitro investigations suggests it is poisonous and carcinogenic to some species of fish. In humans, it irritates the eyes moderately, can permanently injure the cornea and in extreme cases, cause respiratory and kidney failures [15]. Tannins, secondary plant metabolites are non-toxic polyphenols which can leach into the water when used as adsorbents because they are water-soluble. This can be overcome by modifying tannins into various immobile water-insoluble matrices which are inexpensive capable of uptaking heavy metals and dyes from contaminated waters [16–18].

In developing countries like Nigeria, regulatory agencies do little or nothing to stop or control discharging

of contaminated/polluted industrial effluents. Poverty is another important factor that very likely causes industries of most developing nations the inability to put in place facilities for effluent purification [19]. Technologies abound for the treatments of contaminated industrial efflents; however, the use of agricultural solid wastes, involving adsorption processes for purification of wastewaters, now attracts interest because it is effective, efficient, characteristic of low adsorbent regeneration cost, equipment for adsorption processes are easily availabile, economic, easily available and environment-friendly [6,20,21]. It is of uttermost importance to use low cost, easily available and environment-friendly materials as adsorbents for the removal of dye colour and heavy metals from effluents. Agricultural waste materials, such as cashew nut testa tannin resin (CATAR), are known to fulfil these conditions. Valonia tannin resin has been used for competitive sorption of copper, lead and zinc ions from aqueous solutions [22]. Biosorption potentials of modified quebracho tannin resin were reported earlier [23] and the sorption potentials of valonea tannin resin for the removal of palladium (II) and rhodium (III) chloro complexes have been reported [24]. Studies have appeared in the literature for the removal of Brilliant Red (X-3B) using tannin gel [25] and sorption of methylene blue from aqueous solution was earlier reported [26]. Trox and co-workers [27] characterized the phenolic composition of cashew nut testa, amongst other findings; catechin and epicatechin were identified as the phenolic components of cashew nut testa. However, a work [28] characterized the tannins of the testa and the potential applications in leather tanning. Results from the work of Ukoha et al [29] show that tannins of cashew nut testa are mainly condensed, but groundnut husk tannins are mixed (hydrolysable and condensed) revealing the presence of azaleatin, catechin, cyanidin, delphinidin, epicatechin, myricetin and quercetin in cashew nut testa; fisetin, tricin and myricetin in groundnut husk. Nnaji et al [30] reported the use of cashew nut testa tannin aluminium corrosion and an earlier work [19] reported the coag-flocculation potentials of cashew nut testa tannins in industrial effluent purification.

Many countries like Nigeria produce huge amounts of agricultural wastes due to the availability of large vegetation lands, unfortunately in Nigeria, little use of these agricultural waste materials is made [31]. In south-eastern Nigeria, for example, cashew nuts abound and require throwing away the testae generated after processing the nuts for sale [19]. Cashew nut testae are waste materials which have very little or no economic or nutritive value, particularly in Nigeria and contain lots of tannins. Imperatively the use of CATAR as an adsorbent was aimed by this study which reports its novel chemically modification and application in the removal of dyes and metal ions from aqueous solutions.

The development of a low-cost adsorbent from renewable waste was obtained from a plant material by chemical modification of cashew nut testae tannins (CATAR). The effectiveness of the obtained CATAR was tested for the removal of dyes and heavy metals such that the kinetic profiles and thermodynamic parameters (change in free energy, enthalpy and entropy) for the removal processes were determined and discussed.

2. Materials and methods

Details on material preparation are provided in the Supporting Information.

2.1. Methods

2.1.1. Density determinations

Nnaji and co-workers [32] earlier reported the methods followed to determine the bulk, tapped and true densities of CATAR (Supporting Information for details).

2.1.2. FTIR and SEM

Infrared spectra of the adsorbent surfaces before and after immersion in simulated wastewaters were obtained on a SHIMADZU-FTIR-8400S spectrophotometer.

SEM was used to record the images of CATAR before and after the removal of the dyes and metal ions.

2.1.3. Adsorption studies

Stock solutions of dyes and metal ions were prepared by dissolving crystal violet, malachite green, methylene blue, analytical grades of $Pb(NO_3)_2$ (lead nitrate), $CuSO_4.5H_2O$ (copper sulphate pentahydrate) and $Cd(NO_3)_2.2H_2O$ (cadmium nitrate dihydrate) in distilled water.

Batch adsorption experiments were done to monitor the effects of pH, contact time, initial concentration, temperature and adsorbent dosage. Stock standard solutions of metal ions and dyes studied are 1000 mg L^{-1} and were prepared using distilled water. The sets of experiments have a fixed volume of dye or metal ion solutions of 250 mL at the following concentrations: 5, 10, 20, 50, 75, 100, 250 and 300 mgL^{-1}. Adjustment of pH was done using drops of 0.1 M hydrochloric acid or sodium hydroxide solution in the solutions of known initial dye or metal concentrations. After the adsorption period (300 min), the supernatants were taken and centrifuged for 10 min at 3500 rpm, and analysed for dyes using a JENWAY 6405 UV/visible spectrophotometer inter-phased with a computer, but an atomic absorption spectrometer (AAS) was used for analyses of metal ions. Average values of the replicate experiments are presented. Percentage removal was calculated using the following equation:

$$\% \text{ removed } (\%R) = \frac{(C_0 - C_f)}{C_0} \times 100 \qquad (1)$$

Table 1. Some properties of CATAR.

Parameter	Value
Bulk density (g/cm^3)	0.908
Tapped density (g/cm^3)	0.937
True density (g/cm^3)	1.711
Carr's index	3.095
Porosity (%)	33.593
Hausner Index	1.032

where C_0 and C_f are the initial and final concentrations (mg L^{-1}) of dye or metal ion after adsorption, respectively. Adsorption capacity values were calculated using the following equations:

$$q_t = \frac{(C_0 - C_t)v}{m} \qquad (2)$$

$$q_e = \frac{(C_0 - C_e)v}{m} \qquad (3)$$

where C_e and C_t are the equilibrium and time dependent dye or metal ion concentrations (mgL^{-1}), respectively, v is the volume of dye or metal ion solution used (L) and m is the weight of CATAR (g).

3. Results and discussion

3.1. Characterization

Some properties of CATAR are presented in Table 1. Table 1 presents density values of CATAR as follows: 0.908g cm^{-3} (bulk), 0.937g cm^{-3} (tapped) and 1.711 gcm^{-3} (true). The values of true density reported for flax, jute and coir are, respectively 0.180, 1.3 and 1.2 gcm^{-3} [33], value of 1.411 gcm^{-3} is higher for CATAR. True density value of CATAR is 1.711 gcm^{-3}, higher than the value reported for tannin/furanic resin foam with 1.590 gcm^{-3} [34]. Bulk density for corncob has a value of 0.293 gcm^{-3} [35] and the value of 0.908 gcm^{-3} for CATAR is higher. These bulk density values reveal that corncob has lower value than CATAR and imply better sorption properties due to increased internal surfaces [36]. Corncob has a tapped density value of 0.327 gcm^{-3} is less than the value obtained for CATAR, presented in Table 1, 0.937 gcm^{-3} [35].

There is a positive correlation with tapped density material porosity such that better sorption properties are exhibited by materials which are more porous because they contain voids between the particles and the pores within the particles [37]. Corncob has a porosity value of 81.5% which is higher than 33.593% for CATAR [35]. Table 1 presents the porosity value for CATAR.

The surface exchange capacity (SEC) of CATAR was 5.622 mequiv.H$^+$/g, suggesting that it is dominated by ion exchange groups which are predominantly –OH groups [38]. SEC value of CATAR is more than those for other tannin resins derived from *Terminalia arjuna* [39] and valonia [40]. Earlier work [30] reveals that cashew nut testa contains condensed tannins which are extracted and separated as catechin, epicatechin, quercetin, azaleatin, delphinidin and cyanidin [29]. These poly-hydroxyl functional groups are known to chelate metal (II) ions [41]; therefore, they corroborate the use of these as sites for adsorption on adsorbent particles [39].

3.2. Fourier-transform infrared spectroscopy (FTIR) and scanning electron microscopy (SEM)

Infrared spectra of CATAR before and after the adsorption of metal ions are presented in Figure 1(a, b). Analysis of FTIR spectrum of CATAR revealed a broad signal centred at 3392 cm^{-1} due to O–H vibrations [40]. Infrared signals observed in the spectrum of CATAR at 2922 and 2859 cm^{-1} are ascribed to the methylene (–CH$_2$–) bridges formed by reaction with formaldehyde [42,43]. Signals of conjugated C$=$C bonds seen at 1524 and 1400 cm^{-1} are due to aromatic ring vibrations and absorption signal at 1328 cm^{-1} reveals the presence of C–H vibrations. Absorptions at 1200, 1120 and 1100 cm^{-1} indicate the presence of C–O. The proposed assignments for C$=$C, C–H and C–O signals are as proposed by Nnaji and co-workers [19]. There are vibrational signals at 820 and 655 cm^{-1} seen in the spectrum of CATAR, suggesting the presence of substituted aromatic rings and consistent with report elsewhere [19].

On close observation, spectra of CATAR before adsorption and after adsorption of malachite green (CATAR-MG) are very similar, as shown in Figure 1(b); however, there are significant shifts in absorption signals that suggested adsorption took place. Broad absorption and increased intensity due to O-H and N-H signals of poly-phenolic groups, moisture and primary amine, with centre at 3347 cm^{-1} for CATAR shifted to 3392 cm^{-1} for CATAR-MG, suggesting that polyhydroxyl functional groups of CATAR were involved in the adsorption process. This assignment is consistent with earlier proposed assignments [43]. Infrared signals at 2922 and 2859 cm^{-1} (CATAR) ascribed to the methylene (–CH$_2$–) bridges, shifted to 2930 and 2892 cm^{-1}, respectively after the adsorption of malachite green (CATAR-MG). Signals of conjugated C$=$C bonds seen at 1524 and 1400 cm^{-1} for CATAR from aromatic ring vibrations, shifted to 1550 and 1435 cm^{-1}, respectively after the adsorption of malachite green for CATAR-MG. Absorption signal at 1328 cm^{-1} seen in the spectrum of CATAR can be seen to shift to 1349 cm^{-1} after malachite green adsorption in CATAR-MG spectrum, suggesting absorption vibrations are due to C–N [43]. Infrared absorptions of CATAR that suggested the presence of C–O were seen at 1200, 1120 and 1100 cm^{-1}, but these signals shifted to 1235, 1125 and 1108 cm^{-1} after malachite green adsorption for CATAR-MG. These observed shifts found in the spectrum of CATAR-MG, which suggested the adsorption of malachite green by the adsorbent, are proposed assignments for C$=$C, C–H and C–O
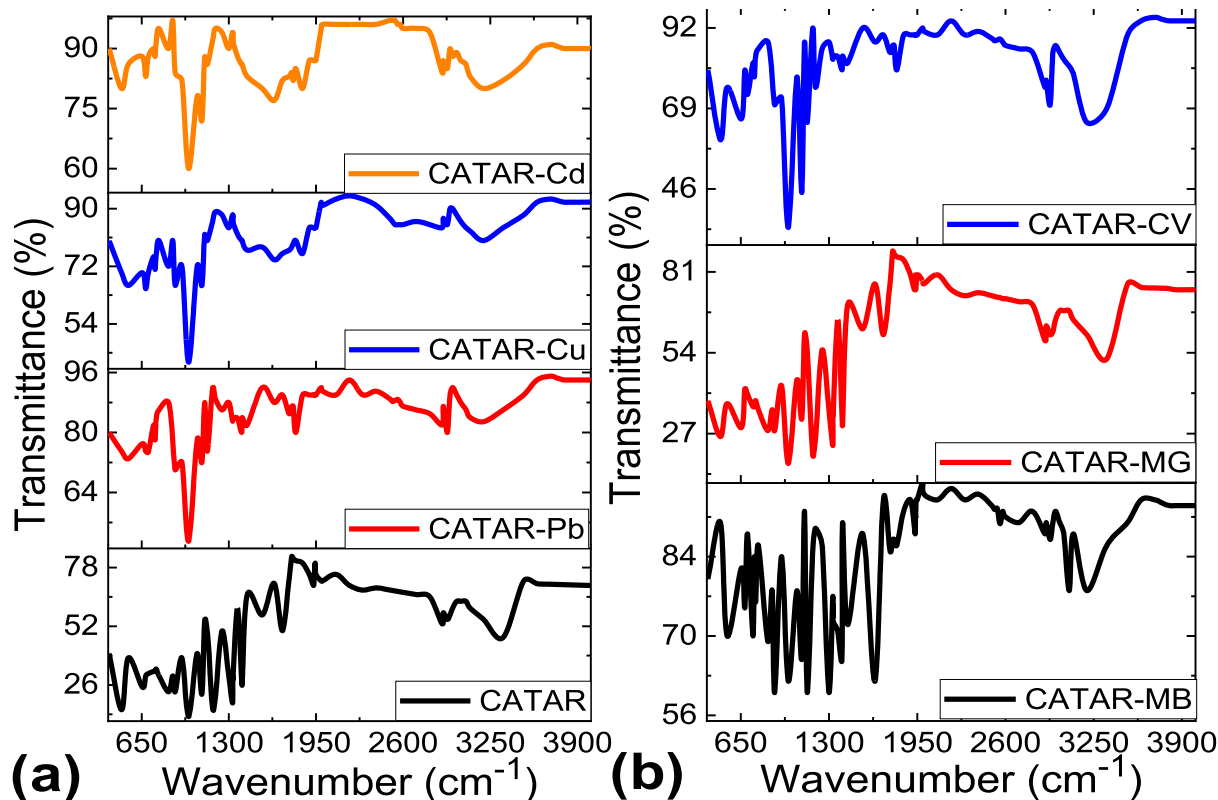
Figure 1. Infrared spectra of adsorbent before CATAR and after adsorption – crystal violet (CATAR-CV), malachite green (CATAR-MG), methylene blue (CATAR-MB), lead (CATAR-Pb), copper (CATAR-Cu) and cadmium (CATAR-Cd).

signals [19]. There are vibrational signals observed in the spectrum of CATAR at 820 and 655 cm^{-1}; these signals shifted after malachite green adsorption to 850 and 667 cm^{-1}, respectively, suggesting the presence of substituted aromatic rings and consistent with report elsewhere [19].

Figure 1(b) presents the infrared spectra of CATAR before and after adsorption of crystal violet (CATAR-CV), significantly different; therefore, suggests adsorption took place. Broad absorption and increased intensity due to O–H and N–H signals of poly-phenolic groups, moisture and primary amine, with centre at 3347 cm^{-1} for CATAR shifted to 3220 cm^{-1} for CATAR-CV, suggesting that polyhydroxyl functional groups of CATAR were involved in the adsorption process. This assignment is consistent with earlier proposed assignments [43]. Infrared signals ascribed to the methylene (–CH$_2$–) bridges were seen at 2922 and 2859 cm^{-1} (CATAR), these shifted to 2926 and 2889 cm^{-1}, respectively after adsorption of crystal violet (CATAR-CV). Signals of conjugated C=C bonds seen at 1524 and 1400 cm^{-1} for CATAR from aromatic ring vibrations, shifted to 1536 and 1457 cm^{-1}, respectively after the adsorption of crystal violet for CATAR-CV. Absorption signal at 1328 cm^{-1} seen in the spectrum of CATAR can be seen to shift to 1368 cm^{-1} after crystal violet adsorption in CATAR-CV spectrum, suggesting absorption vibrations are due to C–N [43]. Infrared absorptions of CATAR that suggested the presence of C–O were seen at 1200, 1120

and 1100 cm^{-1}, but these signals shifted to 1210, 1132 and 1091 cm^{-1} after crystal violet adsorption as seen in CATAR-CV spectrum. These observed shifts found in the spectrum of CATAR-CV and indicated that crystal violet was adsorbed by the adsorbent, are proposed assignments for C=C, C–H and C–O signals [19]. There are vibrational signals observed in the spectrum of CATAR at 820 and 655 cm^{-1}, these signals shifted after crystal violet adsorption to 865 and 650 cm^{-1}, respectively suggesting the presence of substituted aromatic rings and consistent with report elsewhere [19].

The infrared spectra of CATAR before adsorption and after adsorption of methylene blue (CATAR-MB) are presented in Figure 1(b); they are markedly different, which suggests that adsorption took place. An absorption signal due to O–H and N–H signals of poly-phenolic groups, moisture and primary amine, with centre at 3347 cm^{-1} for CATAR shifted to 3206 cm^{-1} for CATAR-MB. This suggests that polyhydroxyl functional groups of CATAR were involved in the adsorption process and the assignment is consistent with earlier proposed assignments [43]. A new peak appears at 3101 cm^{-1} after the adsorption of methylene blue (CATAR-MB) and was earlier ascribed to O-H vibrations of poly-phenolic groups [34]. Infrared signals ascribed to the methylene group vibrations (-CH$_2$-) were seen at 2922 and 2859 cm^{-1} (CATAR) and after the adsorption of methylene blue (CATAR-MB); these shifted to 2937 and 2848 cm^{-1}, respectively. Conjugated C=C
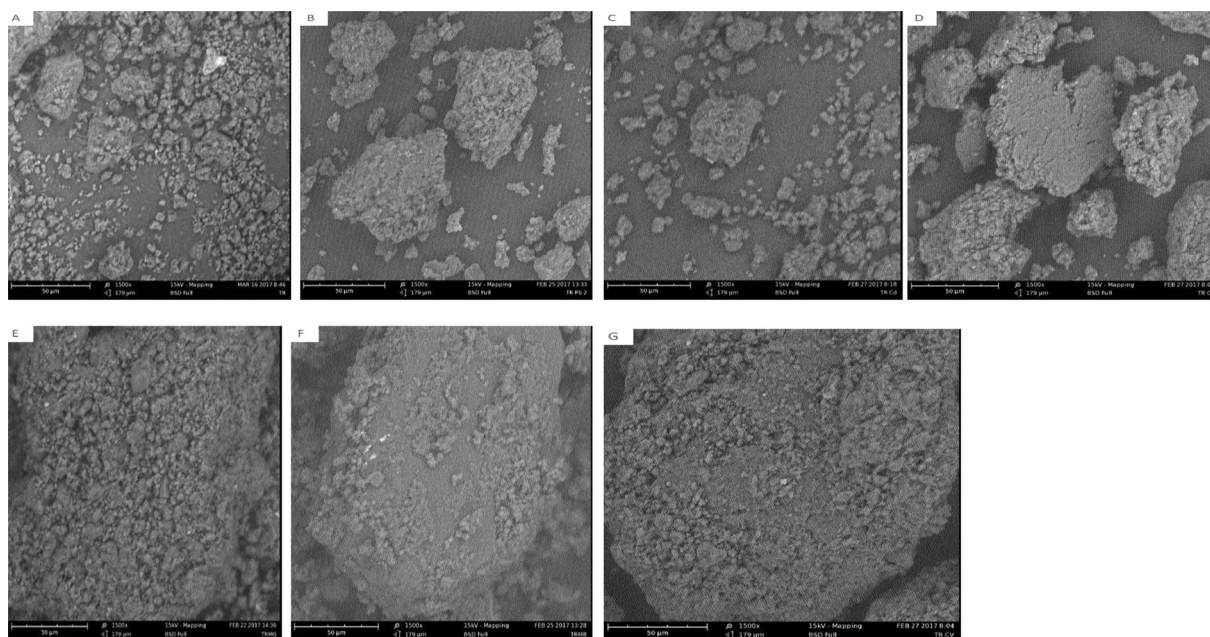
Figure 2. SEM of (a) CATAR; (b) CATAR-Pb; (c) CATAR-Cd; (d) CATAR-Cu; (e) CATAR-MG; (f) CATAR-MB; (g) CATAR-CV.

signals due to aromatic ring vibrations are observed at 1524 and 1400 cm^{-1} for CATAR; these shifted to 1543 and 1472 cm^{-1}, respectively after the adsorption of methylene blue (CATAR-MB). Absorption signal at 1328 cm^{-1} seen in the spectrum of CATAR can be seen to shift to 1365 cm^{-1} after methylene blue adsorption in CATAR-MB spectrum, suggesting absorption vibrations are due to C–N [43]. Infrared absorptions of CATAR that suggested the presence of C–O were seen at 1200, 1120 and 1100 cm^{-1}, but these signals shifted to 1218, 1140 and 1118 cm^{-1} after methylene blue adsorption, as seen in CATAR-MB spectrum. These observed shifts found in the spectrum of CATAR-MB, indicated that methylene blue was adsorbed by the adsorbent, are proposed assignments for C=C, C–H and C–O signals [19]. There are vibrational signals observed in the spectrum of CATAR at 820 and 655 cm^{-1}; these signals shifted after methylene blue adsorption to 860 and 633 cm^{-1}, respectively suggesting the presence of substituted aromatic rings and consistent with report elsewhere [19].

The infrared spectra of CATAR before adsorption and after adsorption of metal ions (CATAR-Cd, CATAR-Cu and CATAR-Pb) are presented in Figure 1(a); they are markedly different, which suggests that adsorption took place. A broad vibrational signal due to O–H of poly-phenolic groups and moisture, with centre at 3347 cm^{-1} for CATAR shifted to 3250, 3198, and 3210 cm^{-1} which corresponds respectively to adsorbed cadmium ions (CATAR-Cd), copper ions (CATAR-Cu) and lead ions (CATAR-Pb). The observed shifts in the infrared vibrational signals after adsorption suggest that polyhydroxyl functional groups of CATAR were involved in the adsorption process. Infrared absorptions

of CATAR, very likely due to the presence of C–O, were seen at 1200–1100 cm^{-1} shifted to 1188–1082 cm^{-1} for adsorbed cadmium ions (CATAR-Cd), 1218–1090 cm^{-1} for copper ions (CATAR-Cu) and 1233–1119 cm^{-1} for lead ions (CATAR-Pb), as seen in Figure 1(a). These observed shifts found in the spectra of CATAR after metal ion adsorption very likely are due to C–O vibrations.

Figure 2(a) presents the SEM micrographs of CATAR surface, revealing a highly heterogeneous surface. It is such that many CATAR particles have different sizes, as shown on the surface of the tannin resin. CATAR surface is rough, as revealed by Figure 2(a), and this is very likely due to tiny surface pores of different CATAR particles. Figure 2(b–g) presents the surfaces of CATAR after the treatment of the wastewaters containing dyes and metal ions. Figure 2(b–g) is SEM micrographs of CATAR surfaces adsorbed with lead (CATAR-Pb), cadmium (CATAR-Cd) and copper (CATAR-Cu) ions; and surfaces of CATAR loaded with malachite green (CATAR-MG), methylene blue (CATAR-MB) and crystal violet (CATAR-CV). After treatment, a distinct change in the surface morphology of CATAR can be observed in Figure 2(b–g). These surface changes seem to aggregate in such a way that dye loaded CATAR surfaces have larger particle than the metal ion loaded surfaces. These are expected considering that the dye molecules are larger than the metal ion siezes, hence the observed morphological differences. These observed differences most likely explain that the removal of the dyes and metal ions from the aqueous solutions became possible due to the likely existence of some interactions between the CATAR surface and molecular matrices of the pollutants (dye and metal ions).
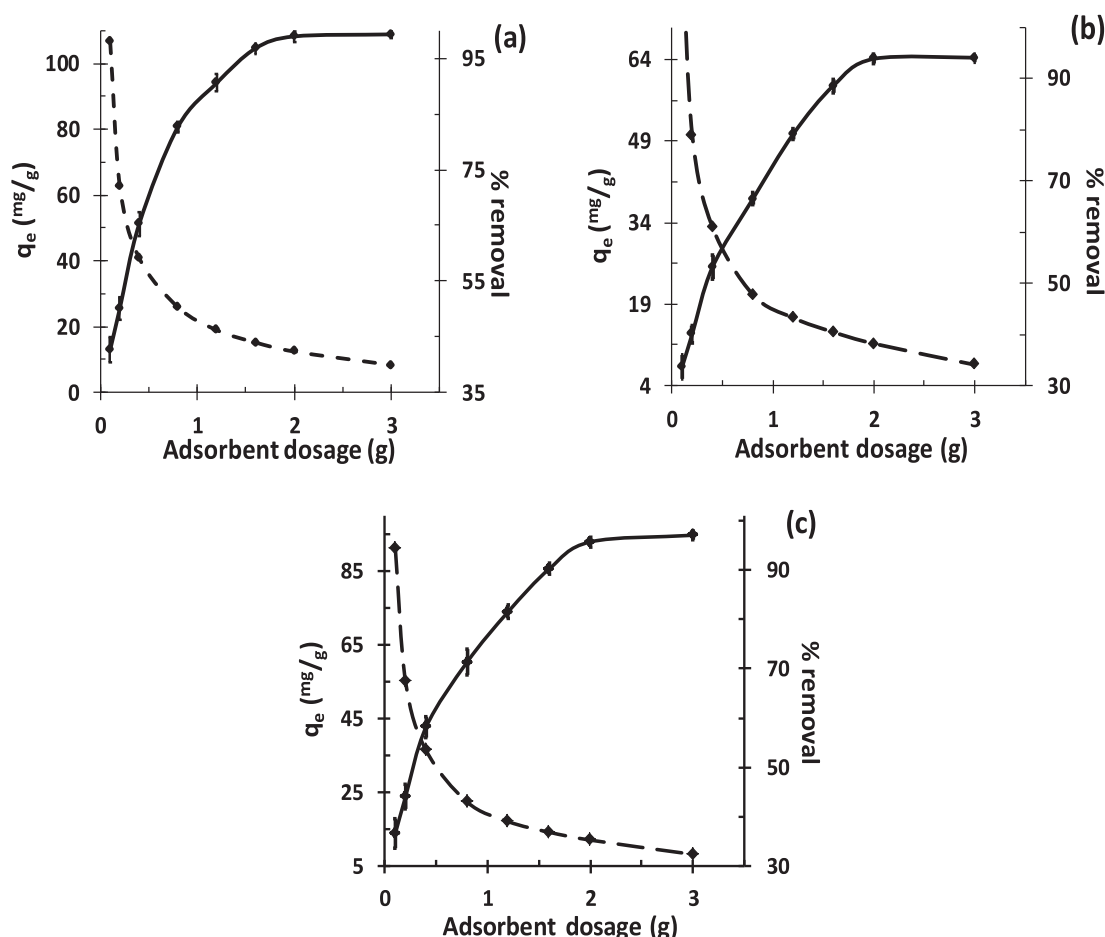
Figure 3. Effect of CATAR dosage on: (a) Cu (II) ion, (b) Pb (II) ion and (c) Cd (II) ion adsorption.

3.3. Effect of CATAR dose

The effect of varying CATAR mass on the adsorption processes was carried out with different adsorbent dosages at the initial concentration of 100 mg.L^{-1}; the volume of solution was kept at 250 mL, at room temperature of 303 K for 2 hrs (Figure 3). The initial pH of 4 was maintained for the simulated wastewaters containing metal ions; however, dye solutions had the initial pH values maintained at 6.

An increase in the removal of metal ions from sloutions was observed to vary/change from 42.6% to 99.4% (copper), 36.5% to 97.1% (lead) and 33.7% to 94.0% (cadmium), as CATAR dosage increased from 0.1 g to 3.0 g. In contrast, the adsorption capacity (q_e) was found to decrease from 106.6 to −8.3 mg.g^{-1} for Cu (II) ion, for Pb (II) ion it decreased from 91.3 to −8.1 mg.g^{-1} and it decreased from 84.3 to −6.3 mg.g^{-1} for Cd (II) ion; adsorption onto CATAR as the amount of the adsorbent increased. A plausible explanation for the increased metal ion removal can be due to increased surface area and availability of more adsorption sites due to the increased adsorbent dose. Similar explanation was posited for observed trends in earlier reports [44,45]. For the observed decrease in adsorption capacity, Unuabonah et al [37] explained that decrease in liquid–solid ratio of CATAR in metal ion solutions (from

0.1 to −3.0 g in 0.25 L) may likely be responsible. Similar observations were made by other researchers. The environmental implication of polluted waters with Cd (II), Cu (II) and Pb (II) ions necessitated a recent study of the effectiveness of chitosan saturated montmorillonite [46] and the present work shows that CATAR has very good metal ion removal potential when compared to mimosa and valonia tannin resins [39].

Figure 4(a–c) presents a trend observed to increase for the removal of studied dye solutions in the following manner: 18.7% to 71.1% (crystal violet), 28.7% to 86.6% (malachite green) and 23.7% to 79.2% (methylene blue), as CATAR dosage increased from 0.1 to 3.0 g. Similar to the adsorption capacity (q_e) trend for metal ions, a decrease was observed from 46.8 to −5.9 mg.g^{-1} for crystal violet, for malachite green it decreased from 71.8 to −7.2 mg.g^{-1} and it decreased from 59.3–6.6 mg.g^{-1} for methylene blue; adsorption onto CATAR as the amount of the adsorbent increased. An account for the increased dye removal can be explained to be caused by increased surface area and the presence of more adsorption sites due to the increased adsorbent dose. Earlier works [44,47] observed similar trends and aforementioned explanation posited. For the observed decrease in adsorption capacity, Unuabonah et al [45] explained that a decrease in liquid–solid ratio of CATAR
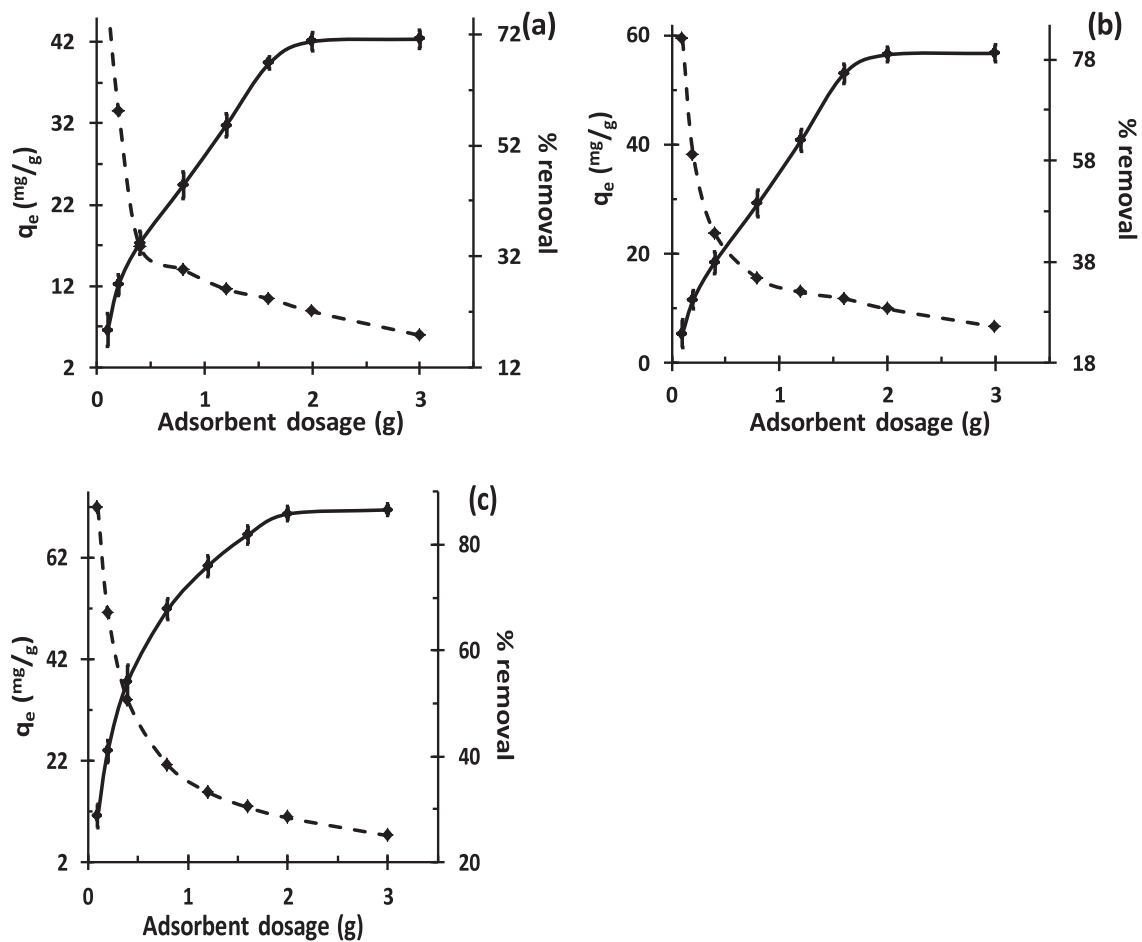
Figure 4. Effect of CATAR dosage on: (a) crystal violet, (b) malachite green and (c) methylene blue adsorption.
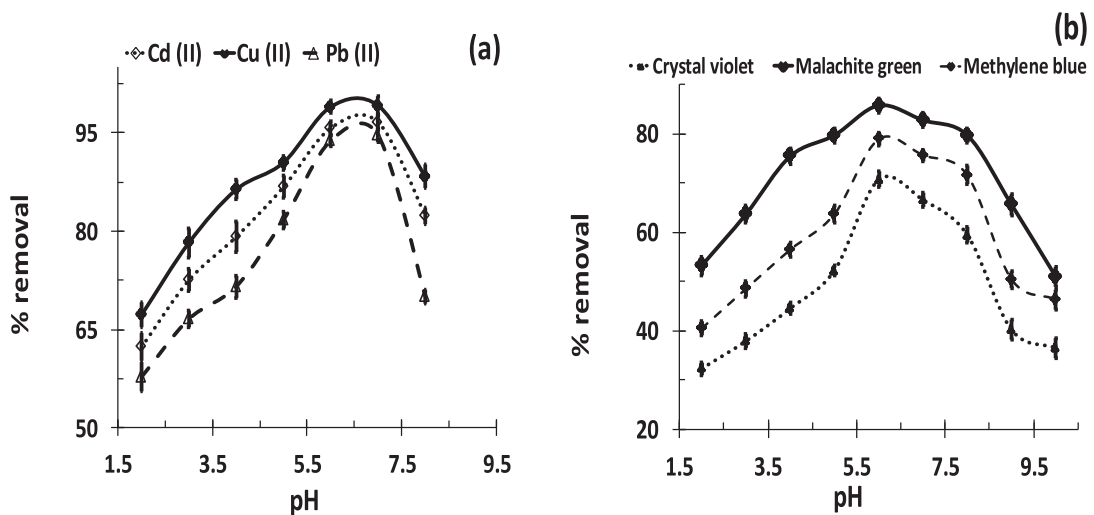
Figure 5. Effect of pH on: (a) metal ion and (b) dye adsorption onto CATAR.

in dye solutions (from 0.1to −3.0 g in 0.25 L) may likely be responsible.

3.4. Effect of pH

Figure 5(a,b) presents the effect of pH on adsorption of metal ion and dye from aqueous solutions onto CATAR, respectively.

The effect of pH on the metal adsorption by CATAR has the removal efficiency values calculated increase with pH as it increases from 2 to 7. A plausible explanation to this observed trend may be due to the acidic dissociation of the phenolic hydroxyl groups of tannin components of CATAR, favouring complex formation by chelating with the metal ions. However, at higher pH conditions, the phenolic hydroxyl groups of the CATAR

would very likely be oxidized more readily and these metal ions precipitate, consequently, removal efficiency of the metal ions decreases. Similar observations have been reported earlier for metal ion adsorption onto tannin resins [47].

Values of percentage dye removal are proportionl to adsorption capacity (not shown) for the adsorption of dye onto CATAR, and were observed to increase with increasing pH from 2.0 to –6.0, but further increase in solution pH from 6.0 to –10.0 caused a decrease in the adsorption trend for dye removal. Figure 5(b) shows that the maximum removal efficiency values are 70.7% for crystal violet, 85.8% for malachite green and 78.9% for methylene blue at pH of 6.0. Surface functional groups on the adsorbent, solution pH, charge of dye molecules and influence of pH on adsorbent surface charge (pH$_{zpc}$) seem to affect the percentage of dye removal from aqueous solutions. Consequently, it is expected that more than an adsorption mechanism may be responsible for dye removal from an aqueous solution by adsorption, but the resultant (or more effective) mechanism is used to explain adsorption process. It is expected that when a solution pH is less than the pH$_{zpc}$ of an adsorbent, it has a net positive surface charge; however, it has a net negative surface charge when a solution pH is more than pH$_{zpc}$. Considering that in aqueous solution, the presence of methylene blue causes it to exist in the form of positively charged ions [48]; therefore, at low pH values, molecules of methylene blue possibly repel with the positively charged CATAR surface, leading to a decrease in dye removal. At increased pH, however, surface functional groups on CATAR seemingly deprotonate due to acidic dissociation of the phenolic hydroxyl groups of tannin causing the CATAR surface to become a negatively charged surface. Increasing the solution pH from 2 to 8, a resultant electrostatic interaction is very likely favoured amongst the positively charged methylene blue dye molecules and the negatively charged CATAR surfaces. These explain the high removal efficiency of the dye molecules by adsorption onto CATAR at pH values equal to or greater than the pH$_{zpc}$ value of 6.04 (shown in supplementary material). Earlier reported results by Boukhemkhem and Rida [49] are in agreement with our findings.

3.5. Thermodynamics of CATAR adsorption

Data were collected at four temperatures from 30°C to 60°C. The quantities of metal ions and dyes adsorbed on CATAR as a function of solution temperature are presented in Table 2. Thermodynamic parameters, such as changes in free energy (ΔG^o), enthalpy (ΔH^o) and entropy (ΔS^o) of adsorption, were determined from the following equations.

$$\Delta G^o = -RT \ln K_D \qquad (4)$$

where $K_D = \frac{q_e}{C_e}$

K_D is the distribution constant of the adsorption process, R is the universal gas constant (8.314 Jmol/K) and T is the solution temperature in K. The changes in enthalpy (ΔH^o) and entropy (ΔS^o) of adsorption were estimated from the slope and intercept of the plot of ln K_D versus T^{-1} as shown in the following equation:

$$\ln K_D = -\frac{\Delta G^o}{RT} = -\frac{\Delta H^o}{RT} + \frac{\Delta S^o}{R} \qquad (5)$$

Table 2 shows that an increase in solution temperature increases the adsorbed quantities of metal ions and dyes. The calculated constants are presented in Table 2 and it can be concluded that the adsorption process was endothermic for the adsorption of metal ions and dyes onto CATAR because change in enthalpy is positive. The changes in free energies of adsorption for the metal ions are negative, suggesting spontaneous adsorption processes. For the adsorption of dyes onto CATAR, changes in free energies of adsorption decreased with an increase in solution temperature, indicating dye adsorption on CATAR was favourable at increased solution temperature. The adsorption processes were accompanied by positive changes in entropy, implying increased randomness, corroborated by rapid adsorption at the solid/solution interfaces. From these results, it can be concluded that adsorption of Cu (II) ion adsorbed most and crystal violet was the least adsorbed caused by the change in solution temperature.

3.6. Adsorption profiles

3.6.1. Kinetic studies
Figure 6 presents the effect of adsorption time on studied metal ion and dye onto CATAR. In the present study, kinetic models were applied to the kinetic profiles of the adsorbing metal ions and dyes.

The adsorption processes onto CATAR almost stopped within 120 min for the metal ions and within 180 min for the dyes. This suggests that metal ions were adsorbed faster than the dyes, considering that the dye molecules are bulkier, as it is supposed. Very fast adsorption occurred within 30 min for the adsorption of metal ions and dyes attaining removal efficiencies of 82.8% for Pb (II) ion, 94.1% for Cu (II) ion, 88.8% for Cd (II) ion, 52.8% for crystal violet, for malachite green it is 74.7% and 66.4% for methylene blue. These correspond to the adsorption capacities of the metal ions: Cu (12.37 mg/g) > Cd (11.97 mg/g) > Pb (11.73 mg/g) and dyes: malachite green (10.72 mg/g) > methylene blue (9.87 mg/g) > crystal violet (8.84 mg/g). It can be inferred that the hydrated ionic radii of the metal ions played vital roles in their adsorption onto CATAR considering that they vary thus: Cu (0.72 Å) < Cd (0.97 Å) < Pb (1.20 Å). This, therefore, implies that the
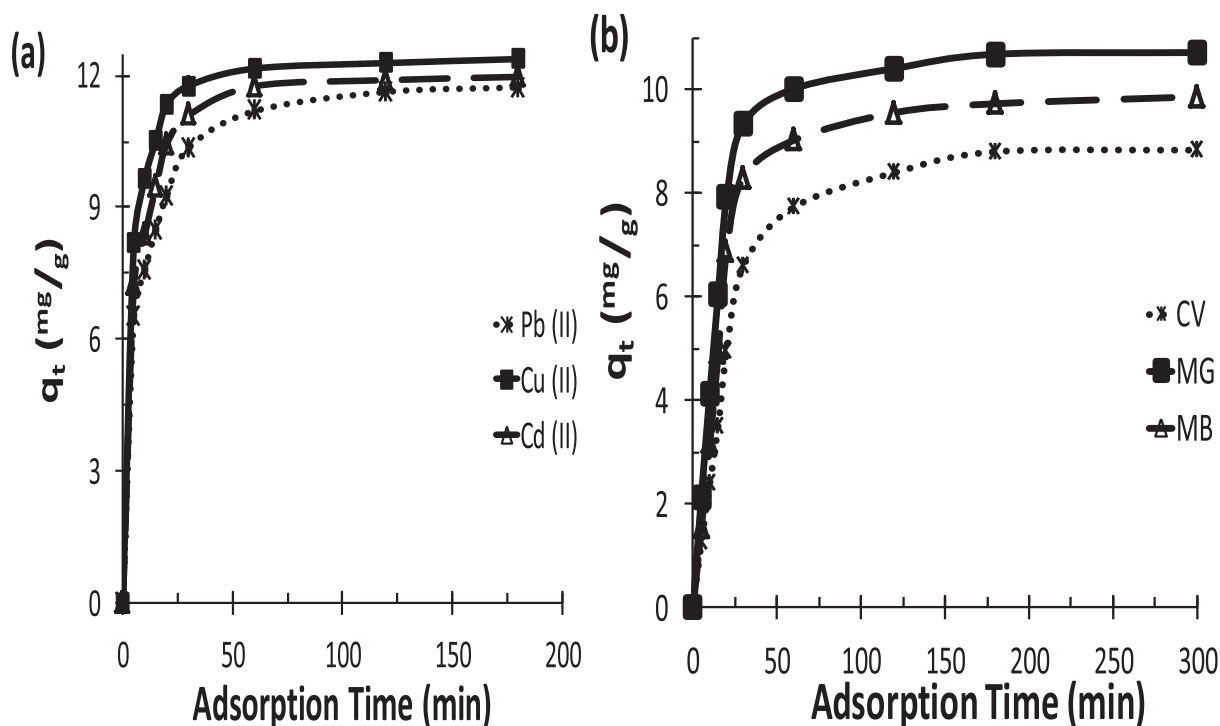
Figure 6. Effect of adsorption time on metal ion (a) and dye (b) adsorption onto CATAR.

Table 2. Thermodynamic parameters of CATAR adsorption.

Pollutant	Temperature (°C)	q_e (mg/g)	K_D	ΔG^o (J/mol)	ΔH^o (kJ/mol)	ΔS^o (JK^{-1}mol^{-1})
Cd (II)						
	30	11.97	22.5	−2604.6	29.5	122.1
	40	12.02	25.8	−3044.0		
	50	12.14	33.3	−3833.0		
	60	12.32	67.4	−5902.2		
Cu (II)						
	30	12.37	12.3	−6317.1	144.0	507.6
	40	12.38	13.2	−6723.1		
	50	12.49	208.2	−14336.3		
	60	12.50	1562.4	−20359.9		
Pb (II)						
	30	11.73	1.9	−1614.7	22.3	95.6
	40	11.80	2.1	−1947.5		
	50	11.99	3.0	−2905.8		
	60	12.13	4.1	−3936.0		
Crystal violet						
	30	8.84	0.30	3020.0	9.2	37.8
	40	9.15	0.34	2802.0		
	50	9.38	0.38	2625.9		
	60	9.64	0.42	2394.1		
Malachite green						
	30	10.72	0.8	712.7	10.3	48.8
	40	10.91	0.9	400.9		
	50	11.07	1.0	88.1		
	60	11.21	1.1	−233.5		
Methylene blue						
	30	9.87	0.47	1910.9	6.9	33.7
	40	10.11	0.53	1665.1		
	50	10.18	0.55	1619.9		
	60	10.37	0.61	1379.9		

smaller the ionic radius of the metal ions, the more the adsorbed specie and this is in agreement with reported findings elsewhere [50]. Removal efficiencies and the corresponding adsorption capacities of the dyes do not seem to follow a consistent trend considering the molecular structures shown in Figure 7. The only exception is that crystal violet has the highest molecular mass

of 407.99 g/mol and has two −N(CH$_3$)$_2$ groups, hence accounts for its calculated least removal efficiency.

Table 3 presents R^2 values for the tested kinetic models and pseudo-second order kinetic model has the highest. This suggests that pseudo-second order kinetics fits the experimental kinetic data of the metal ions and dyes best; however, Figure 8 shows how the tested
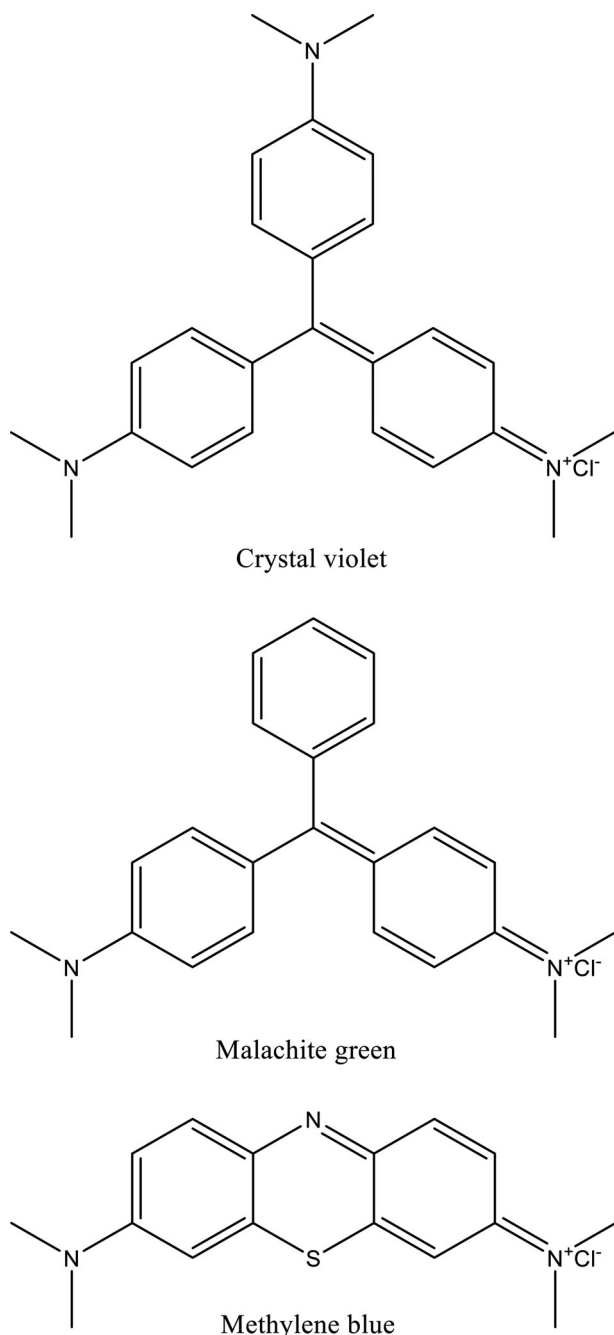
Crystal violet

Malachite green

Methylene blue

Figure 7. Molecular structures of the dyes [51–53].

kinetic models compare with experimental data. Table 3 also presents values of integration constants from intra-particle diffusion plots suggesting that not only one sorption mechanism was involved in the adsorption processes. However, the integration constant values suggest that chemisorption was possibly involved in the adsorption processes [29]. In Figure 8(a–c), the first 5 min seems to follow Elovich, pseudo-second order and intra-particle diffusion kinetics for the kinetic profiles of metal ions, afterwards the pseudo-second order kinetics is followed throughout till 180 min after adsorption. This suggests, therefore, that the metal ions adsorbed onto CATAR external surfaces with quick diffusion into the internal surfaces and adsorbed onto the internal surfaces of CATAR lead to effective removal of the metal ions. In Figure 8(d–f) closely, the first 5 min seem to follow Elovich, pseudo-second order, intra-particle diffusion and liquid film diffusion kinetics for the kinetic profiles of the dyes, afterwards pseudo-second order and liquid film diffusion kinetics were followed at the later adsorption stages. This suggests that the dyes adsorbed onto CATAR external surfaces with quick diffusion into the internal adsorbent surfaces such that the bulkier nature of the dye molecules favoured liquid diffusion mechanism. The kinetic profiles of metal ions and dyes reveal that the effectiveness of CATAR very likely is due to the accessibility of the internal adsorbent surfaces with ease.

3.6.2. Equilibrium studies

The equilibrium isotherms for the adsorption of metal ions and dyes onto CATAR were determined for explaining adsorption equilibrium processes. This study presents three isotherm equations as follows [29,43]:

Langmuir

$$C_e/q_e = \frac{1}{q_0 b} + \frac{C_e}{q_0} \tag{11}$$

Freundlich

$$\ln q_e = \ln K_F + \frac{1}{n} \ln C_e \tag{12}$$

Temkin

$$q_e = B \ln A + B \ln C_e \tag{13}$$

where q_e (mg/g) is the amount of adsorbed specie (metal ion or dye) per unit weight of CATAR and C_e (mg.L^{-1}) represents unadsorbed specie (metal ion or dye) concentration in solution at equilibrium, respectively. Langmuir theoretical saturation capacity is represented by q_0 (mg/g), b is the Langmuir adsorption constant (L/mg), K_F is the Freundlich constant, Freundlich heterogeneity constant is represented by "n", and Temkin constants are represented by A and B. Values of the parameters from the isotherms are presented in Table 4.

The isotherm that fits the experimental data was determined using the regression coefficient (R^2); however, due to the intrinsic predilection caused by linearization, the conclusion from R^2 alone would be erroneous and should be avoided when deciding the applicability of an isotherm model [54]. Often a vital tool for ascertaining the isotherm model best fits experimental data and therefore describes the sorption process is the chi-square statistic (χ^2). The chi-square statistic, Equation (14), is the sum of the squares of the differences between the data obtained experimentally ($q_{e,exp}$) and that obtained by calculation from the isotherm models ($q_{e,cal}$) [31,55], expressed mathematically as follows:

$$\chi^2 = \sum \left[\frac{(q_{e,exp} - q_{e,cal})^2}{q_{e,cal}} \right] \tag{14}$$
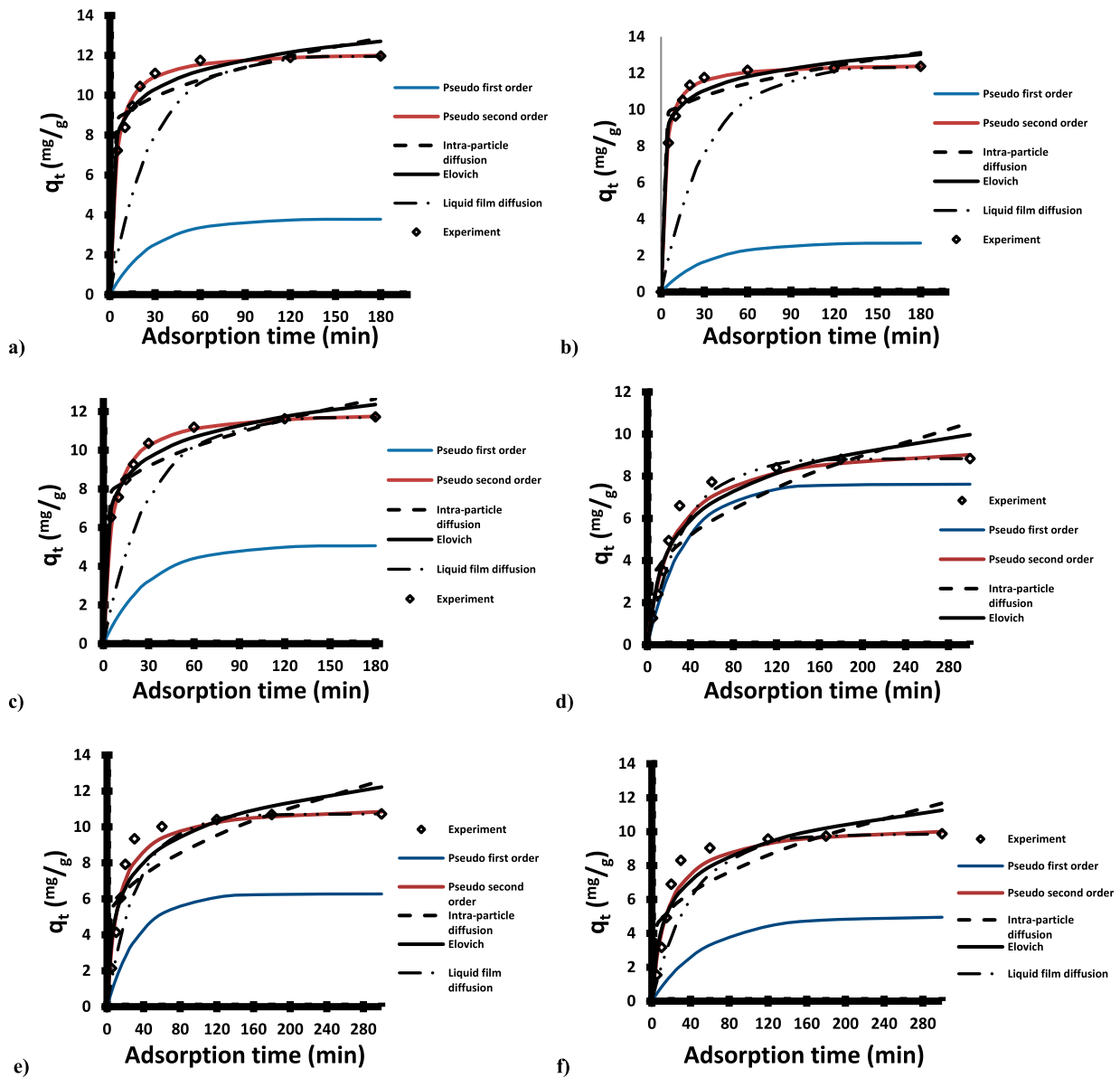
Figure 8. Predicting the kinetic profiles of (a) Cd (II), (b) Cu (II), (c) Pb (II), (d) crystal violet, (e) malachite green and (f) methylene blue onto CATAR.

Calculated χ^2 value would be smaller if the data from the isotherm model are similar to the data from experiment and would be larger if they are different. Values of χ^2 are presented in Table 4. There is a Langmuir dimensionless constant (R_L), otherwise known as separation factor, known to predict biosorption efficiency and can be determined using equation 15 [33]:

$$R_L = \frac{1}{1 + bC_o} \qquad (15)$$

where C_o represents the initial specie (metal ion or dye) concentration. Calculated values of R_L are presented in Table 4. Values of R_L range between $0 < R_L < 1$, reflect favourable sorption process [24]. R_L values for metal ions are smaller than those of dyes such that R_L values calculated for Cu (II) ion are smallest and those for crystal violet are highest indicating that while Cu (II) ion was adsorbed onto CATAR most (and removed best), crystal

violet was adsorbed onto CATAR least (and the least removed).

Langmuir isotherm seems to give the best fit, considering it gave highest R^2 values but χ^2 values calculated are smaller for Pb (II) ion and malachite green equilibrium sorption data. The equilibrium sorption data for Cd (II) ion, Cu (II) ion, crystal violet and methylene blue are best described by the Freundlich isotherm, considering the smallest χ^2 calculated. Temkin isotherm gave the poorest description of the adsorption data, as reflected in the calculated negative χ^2 values.

Methylene blue test is suitable for surface area determination [56] and Equation (16) is the expression herein used for this calculation, as earlier reported [57].

$$\text{Specific surface area (SSA)} = X_m \times N \times A \qquad (16)$$

where the monolayer capacity in moles per gram is represented by X_m (got from the Langmuir isotherm

Table 3. Kinetic parameters of CATAR adsorption.

Model	Metal ion			Dye		
	Cd (II)	Cu (II)	Pb (II)	CV	MG	MB
$q_{e,exp}$ (mg.g^{-1})	11.968	12.374	11.728	8.837	10.722	9.867
Pseudo-first order						
k_1 (mg g^{-1}min^{-1})	0.0363	0.0318	0.0338	0.0288	0.029	0.0183
$q_{e,cal}$ (mg/g)	3.786	2.689	5.076	7.621	6.275	4.968
R^2	0.921	0.8752	0.9813	0.9724	0.9498	0.7990
Pseudo-second order						
k_2 (mg g^{-1}min^{-1})	0.0224	0.0320	0.0151	0.0045	0.0073	0.0059
$q_{t,cal}$ (mg/g)	12.240	12.547	12.107	9.699	11.287	10.537
R^2	0.9999	1.0000	0.9999	0.9950	0.9975	0.9952
Intraparticle diffusion						
k_i (mgg^{-1}min$^{-\frac{1}{2}}$)	0.371	0.299	0.438	0.485	0.480	0.482
C	7.895	9.115	6.782	2.129	4.280	3.326
R^2	0.6955	0.6320	0.7964	0.7544	0.6270	0.6539
Liquid film diffusion						
k_{lfd} (min^{-1})	0.0363	0.0318	0.0338	0.0291	0.0298	0.0237
R^2	0.921	0.8752	0.9813	0.9745	0.9485	0.9164
Elovich						
α (mg/g)	95.185	812.294	27.019	0.956	2.482	1.602
β (g.min.mg^{-1})	0.744	0.905	0.652	0.497	0.481	0.484
R^2	0.8795	0.8341	0.9420	0.9245	0.8402	0.8584

Table 4. Equilibrium parameters of CATAR adsorption.

Model	Metal ions			Dyes		
	Cd (II)	Cu (II)	Pb (II)	CV	MG	MB
Langmuir						
q_0 (mg.g^{-1})	31.153	31.546	28.986	16.611	19.802	17.857
b (L.mg^{-1})	0.212	0.839	0.196	0.070	0.137	0.093
R_L	0.485–0.015	0.192–0.003	0.505–0.017	0.741–0.045	0.593–0.024	0.683–0.035
χ^2	5.442	18.017	2.679	2.470	1.999	2.754
R^2	0.9903	0.9955	0.9925	0.9892	0.9949	0.9932
Freundlich						
K_F (mg·g^{-1})	4.625	8.134	3.913	1.621	2.498	1.992
n (g/L)	2.040	2.397	1.953	2.106	2.157	2.161
χ^2	2.364	5.943	3.889	1.214	3.743	1.781
R^2	0.9856	0.9384	0.9725	0.9831	0.9638	0.9827
Temkin						
B (L.g^{-1})	3.623	4.298	3.797	2.254	2.634	2.352
A (gL^{-1})	13.927	22.074	8.184	2.791	5.483	4.092
χ^2	−1.177	−4.132	−10.073	−0.131	−1.655	−1.001
R^2	0.8272	0.9665	0.9119	0.9202	0.9491	0.9200

that was originally derived for monolayer adsorption), N is the Avagadro number (6.019×10^{23}) and A is the area per molecule on the surface which is 130Å^2 (corresponding to the molecule lying flat on the adsorbent surface). The value of SSA calculated, 43.689m^2/g, is greater than those of silver wattle tannin resin (STR), green wattle tannin resin (GTR) and black wattle tannin resin (BTR) [58]. However, the SSA value obtained for tannin resin derived from Mimosa tannin (MTR), 139.2 m^2/g, is greater than that of CATAR [59]. Comparing the SSA values of CATAR and MTR, the increased SSA values of MTR likely resulted to enhance copper (II) ion adsorption than CATAR.

4. Conclusions

This study presents cashew nut testa tannin resin (CATAR) as a novel adsorbent for the removal of Cd, Cu and Pb ions from aqueous solution with excellent performance, as well as with good property for the removal of crystal violet, malachite green and methylene blue.

Conclusions drawn from this study are summarized as follows:

- CATAR performs optimally at slightly acidic pH
- Pb ion and malachite green adsorption onto CATAR followed Langmuir isotherm and Freundlich isotherm best described Cu and Cd ions as well as methylene blue and crystal violet equilibrium adsorption data best.
- Kinetic studies reveal a complex reaction mechanism because different adsorption stages were revealed for the simulated wastewater adsorption on CATAR.
- Thermodynamics reveal spontaneous and endothermic adsorption processes for the removal of the studied metal ions and dyes.

Apparently, CATAR can be used as an adsorbent for the removal of studied metal ions and dyes from aqueous solution considering its non-competitiveness with food demand, it demonstrated good sorption capacity and availability.

Disclosure statement

No potential conflict of interest was reported by the author(s).

References

[1] Saha U, Fayiga A, Sonon L. Selenium in the soil plant environment: a review. Int J Appl Agric Sci. 2017;3(1): 1–18.

[2] Conrad K, Hansen HCB. Sorption of zinc and lead on coir. Bioresource Technol. 2007;98:89–97.

[3] Ekere NR, Ihedioha JN, Eze IS, et al. Health risk assessment in relation to heavy metals in water sources in rural regions of South East Nigeria. Int J Phy Sci. 2014;9(6):109–116.

[4] Rozada F, Otero M, Moran A, et al. Adsorption of heavy metals onto sewage sludge-derived materials. Bioresour Technol. 2008;99:6332–6338.

[5] Ebokaiwe AP, Omaka ON, Okorie U, et al. Assessment of heavy metals around Abakaliki metropolis and potential bioaccumulation and biochemical effects on the liver, kidney, and erythrocyte of rats. Human Ecol Risk Assess An Int J. 2017. doi: 10.1080/10807039.2017.1410695.

[6] Yagub MT, Sen TK, Afroze S, et al. Dye and its removal from aqueous solution by adsorption: a review. Adv Colloid Interface Sci. 2014;209:172–184.

[7] Prozialeck WC, Edwards JR. Mechanisms of cadmium-induced proximal tubule injury: new insights with implications for biomonitoring and therapeutic interventions. J Pharmacol Exp Ther. 2012;343(1):2–12.

[8] Thomas LDK, Elinder CG, Tiselius HG, et al. Dietary cadmium exposure and kidney stone incidence: a population-based prospective cohort study of men and women. Environ Int. 2013;59:148–151.

[9] Tong S, von Schirnding YE, Prapamontol T. Environmental lead exposure: a public health problem of global dimensions. Bulletin World Health Organ. 2000;78(9): 1068–1077.

[10] Wildman RE, Mao S. Tissue-specific alterations in lipoprotein lipase activity in copper-deficient rats. Biol Trace Elem Res. 2001;80:221–229.

[11] El Safty A, Rashed L, Samir A, et al. Oxidative stress and arsenic exposure among copper smelters. British J Med Medical Res. 2014;4(15):2955–2968.

[12] Taylor AA, Tsuji JS, Garry MR, et al. Critical review of exposure and effects: implications for setting regulatory health criteria for ingested copper. Environ Manage. 2020;65:131–159.

[13] Raval NP, Shah PU, Shah NK. Malachite green "a cationic dye" and its removal from aqueous solution by adsorption. Appl Water Sci. 2017;7:3407–3445.

[14] Albayati TM, Sabri AA, Alazawi RA. Separation of methylene blue as pollutant of water by SBA-15 in a fixed-bed column. Arab J Sci Eng. 2016;41:2409–2415.

[15] Mani S, Bharagava RN. Exposure to crystal violet, its toxic, genotoxic and carcinogenic effects on environment and its degradation and detoxification for environmental safety. In: de Voogt W, editor. Reviews of environmental contamination and toxicology volume 237 (continuation of residue reviews). Cham: Springer; 2016.

[16] Kavitha VU, Kandasubramanian B. Tannins for wastewater treatment. SN Appl Sci. 2020;2:1081.

[17] Kunnambath PM, Thirumalaisamy S. Characterization and utilization of tannin extract for the selective adsorption of Ni (II) ions from water. J Chem. 2015;2015:1–9. Article ID 498359.

[18] Bacelo HAM, Santos SCR, Botelho CMS. Tannin-based biosorbents for environmental applications – a review. Chem Engr J. 2016;303:575–587.

[19] Nnaji NJN, Ani JU, Aneke LE, et al. Modelling the coag-flocculation kinetics of cashew nut testa tannins in an industrial effluent. J Ind Engr Chem. 2014;20:1930–1935.

[20] Crini G, Lichtfouse E, Wilson LD, et al. Conventional and non-conventional adsorbents for wastewater treatment. Environ Chem Lett. 2019;17:195–213.

[21] Barakat MA. New trends in removing heavy metals from industrial wastewater. Arabian J Chem. 2011;4(4): 361–377.

[22] Babel S, Kurniawan TA. Low-cost adsorbents for heavy metals uptake from contaminated water: a review. J Hazard Mat. 2003;B97:219–243.

[23] Sengil IA, Özacar M. Competitive biosorption of Pb^{2+}, Cu^{2+} and Zn^{2+} ions from aqueous solutions onto valonia tannin resin. J Hazard Mat. 2009;166:1488–1494.

[24] Yurtsever M, Sengil IA. Biosorption of Pb (II) ions by modified quebracho tannin resin. J Hazard Mat. 2009;163:58–64.

[25] Can M, Bulut E, Örnek A, et al. Synthesis and characterization of valonea tannin resin and its interaction with palladium (II), rhodium (III) chloro complexes. Chem Engr J. 2013;221:146–158.

[26] Rahman MM, Akter N, Karim MR, et al. Optimization, kinetic and thermodynamic studies for removal of Brilliant Red (X-3B) using tannin gel. J Environ Chem Eng. 2014;2:76–83.

[27] Martin JS, Velasco MG, Heredia JB, et al. Novel tannin-based adsorbent in removing cationic dye (methylene blue) from aqueous solution: kinetics and equilibrium studies. J Hazard Mat. 2010;174:9–16.

[28] Trox J, Vadivel V, Vetter W, et al. Catechin and epicatechin in testa and their association with bioactive compounds in kernels of cashew nut (*Anacardium occidentale*) L. Food Chem. 2011;128:1094–1099.

[29] Ukoha PO, Ejikeme PM, Maju CC. Tannins of the testa of Anacardium occidentale (cashew) and husk of arachis hypogaea (groundnut): Characterisation and potential applications. J Am Lea Chem Assos. 2010;106:242–249.

[30] Nnaji NJN, Obi-Egbedi NO, Okoye COB. Cashew nut testa tannin: assessing its effects on the corrosion of aluminium in HCl. Portugaliae Electrochim Acta. 2014;32(2):157–182.

[31] Akar ST, Yilmazer D, Celik S, et al. On the utilization of a lignocellulosic waste as an excellent dye remover: modification, characterization and mechanism analysis. Chem Engr J. 2013;229:257–266.

[32] Nnaji NJN, Onuegbu TU, Edokwe O, et al. An approach for the reuse of dacryodes edulis leaf: characterization, acetylation and crude oil sorption studies. J Environ Chem Enginr. 2016;4:3205–3216.

[33] Bledzki AK, Gassan J. Composites reinforced with cellulose based fibres. Prog Polym Sci. 1999;24:221–274.

[34] Celzard A, Zhao W, Pizzi A, et al. Mechanical properties of tannin-based rigid foams undergoing compression. Mat Sci Engr. 2010;527(16–17):4438–4446.

[35] Nwadiogbu JO, Ajiwe VIE, Okoye PAC. Removal of crude oil from aqueous medium by sorption on hydrophobic corncobs: equilibrium and kinetic studies. J Taibah Univ Sci. 2016;10(1):56–63.

[36] Angelova D, Uzunovb I, Uzunova S, et al. Kinetics of oil and oil products adsorption by carbonized rice husks. Chem Eng J. 2011;172:306–311.

[37] Ejikeme PM. Investigation of the physicochemical properties of microcrys-talline cellulose from agricultural wastes 1: orange mesocarp. Cellulose. 2008;15 (1): 141–147.

[38] Ozacar M, Soykan C, Sengil IA. Studies on synthesis, characterization and metal adsorption of mimosa and valonia tannin resins. J Appl Polymer Sci. 2006;102:786–797.

[39] Sumathirathne LD, Karunanayake L. Synthesis of novel porous tannin-phenol-formaldehyde cation exchange resin from *Terminalia arjuna* (Kumbuk). J Natn Sci Foundation Sri Lanka. 2017;45(3):219–227.

[40] Şengil İA, Özacar M, Türkmenler H. Kinetic and isotherm studies of Cu (II) biosorption onto valonia tannin resin. J Hazard Mat. 2009;162:1046–1052.

[41] Yu LJ, Shukla SS, Dorris KL, et al. Adsorption of chromium from aqueous solutions by maple saw dust. J Hazard Mat. 2003;B100:53–63.

[42] Mulani K, Daniels S, Rajdeo K, et al. Tannin aniline formaldehyde resole resins for arsenic removal from contaminated water. Canadian Chem Trans. 2014;2(4): 450–466.

[43] Cheriaa J, Khaireddine M, Rouabhia M, et al. Removal of triphenylmethane dyes by bacteria *consortum*. The Scientific World J. 2012;2012:1–9.

[44] Hameed BH. Evaluation of papaya seeds as a novel non-conventional lowcost adsorbent for removal of methylene blue. J Hazard Mater. 2009;162:939–944.

[45] Unuabonah EI, Adie GU, Onah LO, et al. Multistage optimization of the adsorption of methylene blue dye onto defatted carica papaya seeds. Chem Engr J. 2009;155: 567–579.

[46] Hu C, Zhu P, Cai M, et al. Comparative adsorption of Pb(II), Cu(II) and Cd(II) on chitosan saturated montmorillonite: kinetic, thermodynamic and equilibrium studies. Appl Clay Sci. 2017;143:320–326.

[47] Liao X, Li L, Shi B. Adsorption recovery of thorium (IV) by *Myrica rubra* tannin and larch tannin immobilized onto collagen fibres. J Radioanalyt Nuclear Chem. 2004;260(3):619–625.

[48] Doğan M, Abak H, Alkan M. Adsorption of methylene blue onto hazelnut shell: kinetics, mechanism and activation parameters. J Hazard Mat. 2009;164(1):172–181.

[49] Boukhemkhem A, Rida K. Improvement adsorption capacity of methylene blue onto modified tamazert kaolin. Adsorpt Sci Technol. 2017;35(9–10):753–773.

[50] Dawodu FA, Akpomie KG. Simultaneous adsorption of Ni(II) and Mn(II) ions from aqueous solution unto a Nigerian kaolinite clay. J Mat Res Tech. 2014;3:129–141.

[51] Confortin D, Neevel H, Brustolon M, et al. Crystal violet: study of the photo-fading of an early synthetic dye in aqueous solution and on paper with HPLC-PDA, LCMS and FORS. J Phys Conf Ser. 2010;231:012011, doi:10.1088/1742-6596/231/1/012011.

[52] Prabakaran R, Arivoli S. Thermodynamic and isotherm analysis on the removal of malachite green dye using *thespesia populnea* bark. E-J Chem. 2012;9:2575–2588.

[53] Kuang Y, Zhang X, Zhou S. Adsorption of methylene blue in water onto activated carbon by surfactant modification. Water. 2020;12(587):1–19. doi.org/10.3390/w12020587.

[54] Nnaji NJ, Obi-Egbedi NO, Nnabugwu MA. Kinetics and thermodynamics of aluminium corrosion inhibition by anthocleista djalonensis leaf extract in hydrochloric acid solution. Int J Chem Sci. 2012;10(1):182–194.

[55] Nnaji NJN, Okoye COB, Obi-Egbedi NO, et al. Spectroscopic characterization of red onion skin tannin and it's use as alternative aluminium corrosion inhibitor in hydrochloric acid solutions. Int J Electrochem Sci. 2013;8:1735–1758.

[56] Kipling JJ, Wilson RB. Adsorption of methylene blue in the determination of surface areas. J Appl Chem. 1960;10:109–113.

[57] Yukselen Y, Kaya A. Suitability of the methylene blue test for surface area, cation exchange capacity and swell potential determination of clayey soils. Engr Geol. 2008;102:38–45.

[58] Okoli BJ, Shilowa PM, Anyanwu GO, et al. Removal of Pb2+ from water by synthesized tannin resins from invasive South African trees. Water. 2018;10:648, doi:10.3390/w10050648.

[59] Yamaguchi H, Hicasida R, Hicuchi M, et al. Adsorption mechanism of heavy-metal ion by microspherical tannin resin. J Appl Polym Sci. 1992;45:1463–1472.